Acta Materialia 180 (2019) 189–198

Contents lists available at ScienceDirect

Acta Materialia

journal homepage: www.elsevier.com/locate/actamat

Full length article

Swamps of hydrogen in equiatomic FeCuCrMnMo alloys: First-principles calculations

X.L. Ren [a], P.H. Shi [a], W.W. Zhang [a], X.Y. Wu [b], Q. Xu [c], Y.X. Wang [a, *]

[a] Key Laboratory of Nuclear Physics and Ion-beam Application (MOE), Institute of Modern Physics, Department of Nuclear Science and Technology, Fudan University, Shanghai, 200433, China
[b] The First Sub-Institute, Nuclear Power Institute of China, Chengdu, 610005, China
[c] Research Reactor Institute, Kyoto University, Kumatori-cho, Sennan-gun, Osaka, 590-0494, Japan

ARTICLE INFO

Article history:
Received 15 March 2019
Received in revised form
5 September 2019
Accepted 10 September 2019
Available online 12 September 2019

Keywords:
Ab initio calculations
Molecular dynamics
Monte Carlo method
Hydrogen diffusion
Diffusion mechanism

ABSTRACT

High-entropy alloys (HEAs) merit promising applications in nuclear reactors. A FeCuCrMnMo HEA with low activation under neutron irradiation was studied, which was first focused on the search of an equilibrium state by a hybrid method combining the Metropolis Monte Carlo method and density functional theory (DFT). As a transmutation byproduct in fission reactions or fuel for fusion reactions, the evolution of hydrogen, in the HEA was then investigated through a systematic analysis of H solution and diffusion using DFT and molecular dynamics simulations. Rooted in the unique distortion of HEA lattices, i.e., the destroyed translational symmetry of the energy landscape, tetrahedral and octahedral interstitial positions have no significant difference in the priority of H residing. Diffusion of H, as a guest atom, also presents a sluggish effect. The dramatic increases and decreases in potential energy generate a great number of insurmountable barriers pervading the matrix and largely suppressing the mobility of H. However, this effect originates not only from the difference between the potential energies of interstitial positions as observed with host atoms, which increases the fluctuation of migration barriers and decreases the effective atomic jump frequency, but also from the destabilization of interstitial positions for H residing. This blocks the diffusion channels of H and further decreases the atomic jump probability in Einstein's equation. The present investigation provides fundamental insight into H behavior in HEAs and clues for the application of HEAs as materials of tritium permeation barriers or resistance to hydrogen irradiation.

1. Introduction

Incorporating multiple elements into single-phase solid solutions can effectively increase the radiation tolerance of the resulting materials [1–6]. Recent experiments revealed that, compared to pure nickel, NiCoFeCr alloy can suppress void formation by two orders magnitude at elevated temperatures [7]. It is suggested that the limited mobility of large vacancy clusters plays an important role in suppressing cluster growth [8]. Additionally, the migration of self-interstitials is also suppressed and leads to enhanced point defect recombination, indicating a self-healing feature under heavy-ion irradiation conditions [9,10]. Up to now, a thorough evaluation concerning the irradiation tolerance of high-entropy alloys (HEAs), which is crucial for the safe operation of nuclear reactors, is still lacking, because the issues under irradiation of light ions originating from transmutation byproducts remain unexplored. In particular, the profound physics beneath the phenomenological descriptions of these light ions in the disordered chemical environment of HEAs is urgently required to be revealed. However, intensive studies on the sluggish effect just focused on host atoms in HEAs [7,10–15]: fluctuations in local lattice potential energy [11], increased migration barriers, decreased jump frequencies [12,13], correlation effects [10,14], and the retention of nanocrystals [15] have been found to be responsible for the anticipated sluggish diffusion in HEAs. As significant invading elements in nuclear environments, the evolution of light ions, such as hydrogen, in HEAs is an intriguing issue.

Light elements, such as hydrogen isotopes, from transmutation byproducts or high-heat particle flux from plasma, accumulate to great extent in the matrix and lead to mechanical and physical

* Corresponding author.
E-mail address: yxwang@fudan.edu.cn (Y.X. Wang).

https://doi.org/10.1016/j.actamat.2019.09.014
1359-6454/

failure of materials. Examples of this include H-induced embrittlement in steels and blistering on tungsten surfaces caused by deuterium [16,17]. Information about the mobility and retention of H isotopes are of great concern in these issues. It has been revealed that H atoms exhibit low solubility and high mobility in traditional metals [18–21]. Solute H atoms are almost immobilized at defect sites after permeating the surface, promoting the formation of H bubbles in traditional metals [22]. Given the deleterious damage to materials caused by H irradiation, it is of great interest to investigate the absorption and diffusion behaviors of H when exploring the applications of HEAs in the nuclear industry.

To date, most of the HEAs studied for potential application in the nuclear industry have been composed of Cr, Mn, Fe, Co, and Ni principal metallic elements. Studies have demonstrated that the Cr–Mn–Fe–Co–Ni system has a small mean free path of electrons and high irradiation tolerance because it exhibits the common features of the HEAs, such as high distortion of lattice and chemical complexities [23]. However, Ni and Co (especially Co) exhibit high activation under neutron irradiation. Therefore, Fe–Cr–Cu–Mn–Mo system alloys excluding high-activation Co and Ni were studied by Xu Q et al. [24], whose structure was well fitted with the BCC structure model by the X-ray diffraction pattern.

At present, an increasing body of experimental evidence suggests that, short-range order (SRO) can emerge in HEAs, e.g. the Cu-containing HEAs [25]. SRO emergence is dependent on temperature [26,27]. SRO in HEAs has been treated as a weak perturbation of chemical disorder, and has thus been nearly neglected in previous theoretical studies. Currently, two methods stand out in the theoretical research community. The first method is supercell approximation, in which the periodic boundary condition is artificially imposed on the supercell to create a disordered configuration. Typically, the special quasirandom structure (SQS) method [28], has been used to mimic the local pair and multisite correlation functions to approach a fully random state mathematically. The second method is the effective medium, where each atom in the lattice is assumed equivalent and embedded in a uniform average medium. One example of this is the virtual crystal approximation (VCA), in which the alloy is assumed to possess atoms of a single type obtained from the weighted average of species concentrations, as well as the coherent potential approximation (CPA) [24,29]. CPA is to some extent a VCA scheme improved through modifying the atomic potential, and inhomogeneous CPA has been developed [30], which is able to deal with SRO in multicomponent metallic alloys. Predicting a stable phase structure is still a crucial step in the HEA-design strategy for both theories and experiments. In fact, it is a significant challenge to quantify the structural nature of HEAs and correlate the structure with the properties of HEAs.

Motivated by the excellent radiation resistance of HEAs, inspired by the intriguing features of the atomic arrangement, and using the equiatomic FeCuCrMnMo alloy as a case study, we developed a methodology combining the Metropolis Monte Carlo (MMC) method [31] and density functional theory (DFT). This allows searching for phase stability [27,32,33], to investigate the chemical ordering of atomic arrangement and its impact on the evolution of H in HEAs. It was found that the solution energies of a H atom, which are converged at a single value in a pure or dilute metal, exhibit diverse values in the interstitial positions of the same species. The discrepancy of the values is even enlarged to 0.56 eV. Octahedral interstitials (OIs) are more stable overall than tetrahedral interstitials (TIs) for H residing, which is uncommon in BCC metals. With the origin rooted in the disordered chemical environments and unique site-to-site lattice distortions of HEAs, the energy barriers to diffusion and the effective jump frequency, as well as the kinetic trajectories of H atoms are investigated to provide deep insight into the sluggish diffusion occurring not only to self-interstitials, but also to guest H atoms in HEAs.

2. Calculation method

2.1. The hybrid MMC/DFT method

A MC/DFT code has been developed by Ghazisaeidi and coworkers [33], which works in the Gibbs semi-grand ensemble, allows to predict the accurate equilibrium phases, whatever the number of components and whatever the crystallographic structures. We constructed a hybrid method that combines MMC and DFT. The MMC method is widely used for searching for equilibrium states of liquids and solids along a Markov chain. Because DFT is included in this methodology, the advantage of MMC/DFT is rooted in its comprehensive consideration of atomic physical properties on the electronic scale. Here, an equiatomic system with five principal elements was predicted in the isothermal-isobaric ensemble (NPT) with a constant number of total atoms, where the required energy of the system was provided by a DFT calculation. Molecular dynamics (MD) calculation based on semi-empirical potentials of atomic interaction can also provide the system energy, where the potential is usually fitted by the parameters of the system, such as the lattice constant, the cohesive energy, the elastic constants, the vacancy formation energy and the stacking fault energy. To our best knowledge, there are no reliable interatomic potentials able to accurately describe the properties of the FeCuCrMnMo alloy because of its complication. DFT merits to be used in the energy calculation for its superior accuracy and predictive capability.

The hybrid MMC/DFT is a self-compiled code. The algorithm primarily follows trials for each MMC step: (1) site exchange in one randomly chosen pair of different species creates a new configuration; (2) based on the configuration after exchanging, the system energy is obtained by DFT with dirty convergence; (3) an acceptance of a new configuration is decided according to the relation of probability according to the standard Metropolis method as follows: $P_{new}/P_{old} = \exp\{-\Delta U/kT\}$, where kT is the Boltzmann factor and ΔU is the energy difference of systems between the old state (before site exchange) and the new state (after site exchange). If P_{new}/P_{old} is larger than 1.0, the new state is accepted; otherwise, the new state is accepted within the probability P_{new}/P_{old}. The details and validation of this method can be found elsewhere [32,33].

In principle, the simulation cell should be set as large as possible because chemical disorder characterizes HEAs. However, thousands of MMC steps were required for searching an equilibrium state. This imposes extremely high computational costs and requires long CPU time, such that we have to choose an appropriate size of simulation cell. We examined the size convergence of the simulation cell. A $2 \times 2 \times 5$ supercell with 40 atoms, $2 \times 3 \times 5$ with 60 atoms, $3 \times 3 \times 5$ with 90 atoms, and $5 \times 5 \times 5$ primitive cells with 125 atoms have been chosen to calculate the chemical disorder for comparison. Eventually, an intermediate supercell with 90 atoms was considered. It was proven to be effective in the following calculations. Using this method, the final configurations we obtained are independent of the initial configurations.

2.2. DFT calculations

The DFT calculations were performed using the VASP code. The exchange-correlation functional was selected as generalized gradient approximations (GGA) determined by Perdew–Burke–Ernzerhof (PBE), which has been proved as the best approach to describe magnetic materials [34]. The $3 \times 3 \times 5$ super cell with 90 atoms was selected in simulations.

During the search for the equilibrium state along the Markov chain, the dirty convergence of DFT calculation is: the energy cut-

off is 330 eV, Γ-centered grid is selected for faster convergence, the energy convergence is 0.1 meV and a force convergence criterion is 20 meV/Å. After each accepted exchange, the configuration was fully relaxed. At the equilibrium stage of the MMC/DFT, the resulting changes are of the order of 5 meV per atom, a value that we consider small compared to the gain obtained from chemical ordering, which typically is ten times larger. The DFT calculation is something like the fast calculation in the work [35]. When we obtained an equilibrium configuration from MMC, we further optimized the configuration with more accurate convergence criteria in order to carry out electron calculations and H evolution study: the plane-wave energy cutoff was taken as 350 eV, nearly 1.3 times higher than the default value for Cu; the energy convergence criterion was taken as 10^{-5} eV; K-points with $4\times4\times 2$ were used. AIMD calculations were performed at the Γpoint only with energy cutoff of 350 eV and energy convergence of 0.1 meV. The canonical NVT ensemble was set in AIMD simulation with the time step taken as 2 ps A spin-polarized scheme was considered in all calculations. Additionally, the SQS structures were built using alloy theoretic automated toolkit (ATAT) codes [36] to mimic the fully random state of the alloy with multiple principal elements, to compare the structure and properties of the HEA alloy obtained from MMC/DFT. Six SQS structures were used to estimate the total energy of the HEA lattice in random state. The order parameters of the nearest-neighbor atomic pairs in the quinary SQS lattices are all closed to zero, which are illustrated in Figs. S1 and S2 of the Supplemental Material.

The climbing-image nudged elastic band (CI-NEB) method [37,38] was used to investigate the diffusion barrier of H interstitial atoms. To calculate the migration barrier, the initial and final positions for H jumping should be stable, which can be obtained via fully optimizing the two configurations. Three or more intermediate structures are interpolated along the pathway and connected like a “spring band” to search the minimum energy path (MEP). After optimizing, one of the intermediate points always climbs right to the saddle point to precisely predict the activation energy. The vibration frequency of the interstitial atom in the saddle point exhibits only two real frequencies, which is the feature of the saddle point. The method to calculate the frequencies accords to finite difference method [39].

2.3. Short-range order parameter

To characterize the chemical ordering of the HEA, we adopted an SRO parameter for the atomic site with respect to a given species i atom, defined by Cowley [40] as follows:$\alpha_{ij}^{n}=1-p_{ij}^{n}/x_j$, where P_{ij}^{n} is the probability that the atomic site is occupied by atomic species$j$ around the given i atom in the nth neighboring shell (here, we chose n = 1) and x_j is the proportion of type$j$ in the alloy. α_{ij} is the ensemble average after reaching the equilibrium state. $\alpha_{ij}=$ 0corresponds to a fully disorder state; for $\alpha_{ij}>0.0$, i–j pairs are smaller than those in a fully random structure; $\alpha_{ij}<0.0$, i–j pairs become more numerous, indicating that species j atoms precipitate around type i.

2.4. Solution energy of H in HEA

The solution energy is calculated using:

$$E_{bulk}^{S}=E_{bulk+\mathrm{H}}-E_{bulk}-1/2E_{\mathrm{H}_2}, \quad (1)$$

where$E_{bulk}$and$E_{bulk+\mathrm{H}}$are the total energies of relaxed configurations of the perfect lattice and the lattice embedding one H atom, respectively. $E_{\mathrm{H}_2}$is the chemical potential of H_2 in the gas phase. $1/2E_{\mathrm{H}_2}$is −3.37 eV, which is consistent with previous results [21].

3. Results

3.1. The structure of the HEA

The hybrid MMC/DFT method was performed to search for the lattice equilibrium state of an equiatomic FeCuCrMnMo alloy. The simulation started from a SQS structure with the initial lattice parameter (a_0) from the experiment, 2.878 Å [24]. When the energy deviation between sequential acceptance states is smaller than 5 meV/atom, we considered the Markov chain is converged. At 800 K, 3000 MC steps were performed until the system approached thermodynamic equilibrium and the corresponding lattice parameter (a) could be obtained as shown in Table 1. Meanwhile, the SRO was monitored, as shown in Fig. 1. It has been proved that SRO would be generated in HEAs under thermal treatment or radiation conditions [10,41]. For comparison and analysis, the SQS structures of the FeCuCrMnMo system and the corresponding pure metals were calculated, all the results of which are listed in Table 1. The calculated results of pure metals are in good agreement with previous work.

The structure obtained from the MMC/DFT method (named SRO structure hereafter for convenience) is more compacted and has lower energy by 35 meV per atom with respect to the fully random structure from SQS, indicating that the existence of SRO favors the energy stability of the system. As shown in Figs. S3–S5 (the Supplemental Material), SRO is related with the temperature. With increasing temperature, the SRO curves move towards the random state. The average value of the Cu–Cu pair equals −0.53 at 800 K, indicating that a Cu-rich region is formed. The result is in accordance with previous experimental observations, where the Cu

Table 1
Cohesive energy per atom, structural volume per atom, and lattice parameters for SRO and SQS structures, and Fe, Cu, Cr, Mn, Mo, and W metals. FM, AFM, and NM denote ferromagnetism, antiferromagnetism, and nonmagnetic, respectively.

System	State	Lattice	Cohesive energy (eV)	Volume (Å^3)	Lattice Parameters	
					a	a_0 (Expt.)
Fe	FM	BCC	−8.32	11.78	2.832	2.834 [19]
Cu	NM	FCC	−3.72	11.81	3.636	3.615 [42]
Cr	AFM	BCC	−9.51	11.97	2.835	2.882 [42]
Mn	FM	BCC	−8.29	14.38	3.080	3.080 [42]
Mo	NM	BCC	−10.95	15.58	3.148	3.147 [42]
W	NM	BCC	−13.01	15.85	3.169	3.171 [22]
$HEA_{\_SQS}$	FM	BCC	−8.09	12.53	2.926	2.878 [24]
$HEA_{\_SRO}$	FM	BCC	−8.13	12.15	2.896	
	NM	BCC	−8.12	12.05	2.889	
	FM	FCC	−8.08	12.31	3.666	

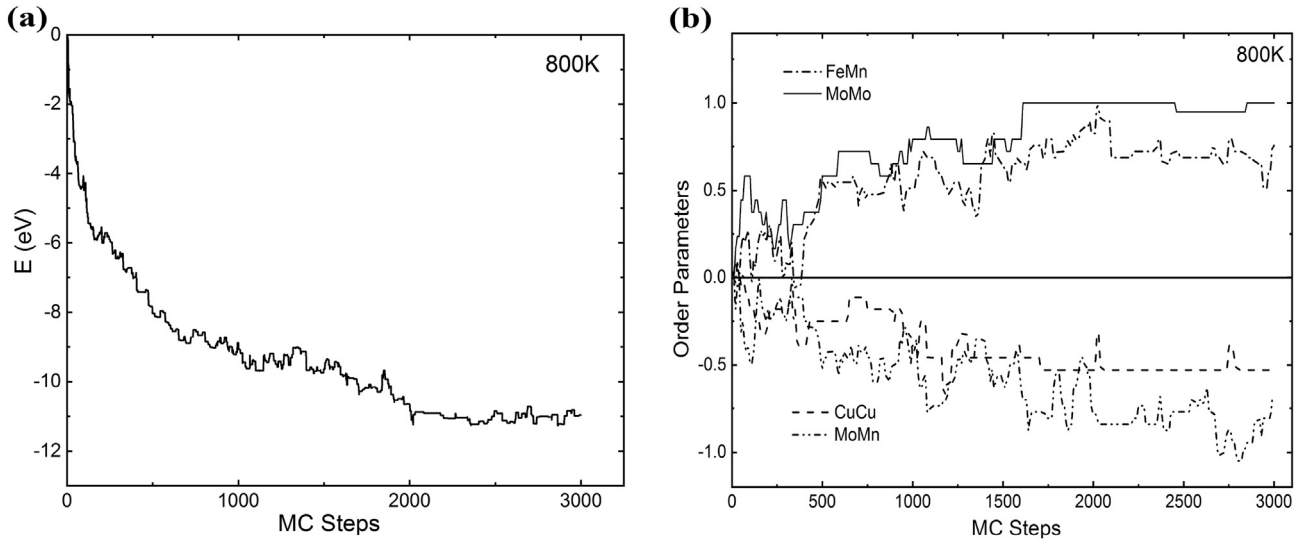

Fig. 1. System evolution vs MC steps at 800 K. (a) System energy; (b) SRO parameters for atomic pairs. System evolution at 1000 K, 1200 K, and 1500 K are all illustrated in Figs. S3–S5 of the Supplemental Material.

segregation was probed through positron annihilation spectroscopy (PAS) after annealing [24]. The Cu aggregation is attributed to large mixing enthalpy of Cu with other species. Because the SQS method is merely a mathematical approximation to the fully random state, the atomic size, interatomic preferential combination, and other factors are ignored in the alloy design of the SQS. The random-structure system energy was estimated from averaging six random configurations. Moreover, the SRO structures in the non-magnetic (NM) state and a FCC lattice were also calculated for comparison. The results verified that the SRO structure with BCC lattice in ferromagnetism (FM) exhibited the most stable state. Hence, we focused on the SRO structure of 800 K to study the evolution of H in the FeCuCrMnMo alloy. It should be borne in mind that even though the lattice crystal undergoes chemical short ordering, overall disorder remains in the whole bulk.

3.2. Electronic distribution in the HEA

Fig. 2 shows the distribution of electron density. It is obvious that the distribution of electron density is no longer uniform over all the interstitial positions. Electrons are notably sparse in the region of Cu aggregation, compared to other interstitial sites outside of Cu aggregation. The enrichment of Cu facilitates the forming of few-electron wells, because the Cu atom has a full d shell with fairly inactive valence electrons and its nearby electron density is to some extent depleted. The electron density of Cu and Fe atoms exhibits a quasi-spherical shape, which indicates typical ($t_{2g} + e_g$)-like orbitals, rather than the quadrilateral distribution found in Mo, Cr, and Mn atoms due to their (a)-like orbitals [43].

3.3. Solubility of H interstitial of HEAs

In traditional metals, the potential isosurface and electrons consistently exhibit periodic distributions, with the periodic arrangement of lattice atoms. Every interstitial position, as a high-symmetry point, could stably accommodate light interstitials, such as H, and the solution energy in each equivalent symmetry position is the same. However, in the HEA, the lattice and the potential isosurface of electronics distortions illustrated in Fig. 3 and the chemical environment diversity break the high symmetry of the lattice, such that all the OI/TI positions are no longer equivalent, which causes many of the OI/TI positions to be unlivable for light atoms from an energetic viewpoint.

Because the chemical environment is heterogeneous over the interstitial positions in HEAs, nearly fifty random selected interstitial sites were sampled, including OIs and TIs, to study the solubility of H in the Fe–Cr–Cu–Mn–Mo HEA. Some of these sites are symbolized as crosses in Fig. 2. Fig. 4 shows that the H solution energy splits into multiple values whenever H is in OI or TI positions, rather than a single value as in a pure metal or dilute alloy. As shown in Table S1 of the Supplemental Material, the electron density is related to the coordinate of the elements, or in other words, the chemical environment. In addition, the difference in the solution energies between OI and TI is not evident in the HEA. It seems that OI is slightly superior to TI for H residing as a whole. The average solution energy in TI (0.401 eV) is larger than that in OI (0.228 eV). This case is different from that in pure BCC metals, such as iron and tungsten [18,19], where TI is a favorable position for H. Here, the zero-point energies (ZPE) were calculated as $E_{ZEP} = 1/2 \sum h\nu$. The following analysis considers the ZPE corrections.

According to the previous reports, in the evolution of H in homogeneous electronic gas, and particularly, in a tungsten bulk, a H atom would prefer to stay in a position with an appropriate electron density when trapped by a vacancy. If the space density exceeds (a)e/Å^3, the relationship between the H solution energy and electron density is monotonically positive [44,45], i.e., it is energetically unfavorable for H to reside at a high-electron-density position. In the HEA, the interstitial positions with similar coordinate environments and electron density, e.g., the pairs of OI1/OI2, OI3/OI4, and TI1/TI2, exhibit diverse values of solution energy (see Fig. 4). Furthermore, a low-electronic-density region is indicated by a square in Fig. 2b to study the relationship between the electronic density and the solution energy in detail. In the square, there are nine OI and TI sites numbered, where Site 1 is OI4 of Fig. 2a. Only two of them (Site 1 and Site 2) are energetic stable in the HEA with solution energies of 0.003 and 0.099 eV, respectively, because H spontaneously moves from the other seven positions into OI4 during optimization. However, the electron density at Site 1 is not the lowest, again reflecting that the H solution energy and the electron density do not exhibit a monotonically increasing relationship. Simple metals have high translational symmetry. All the TI (OI) sites are equivalent, having the same coordinate environment

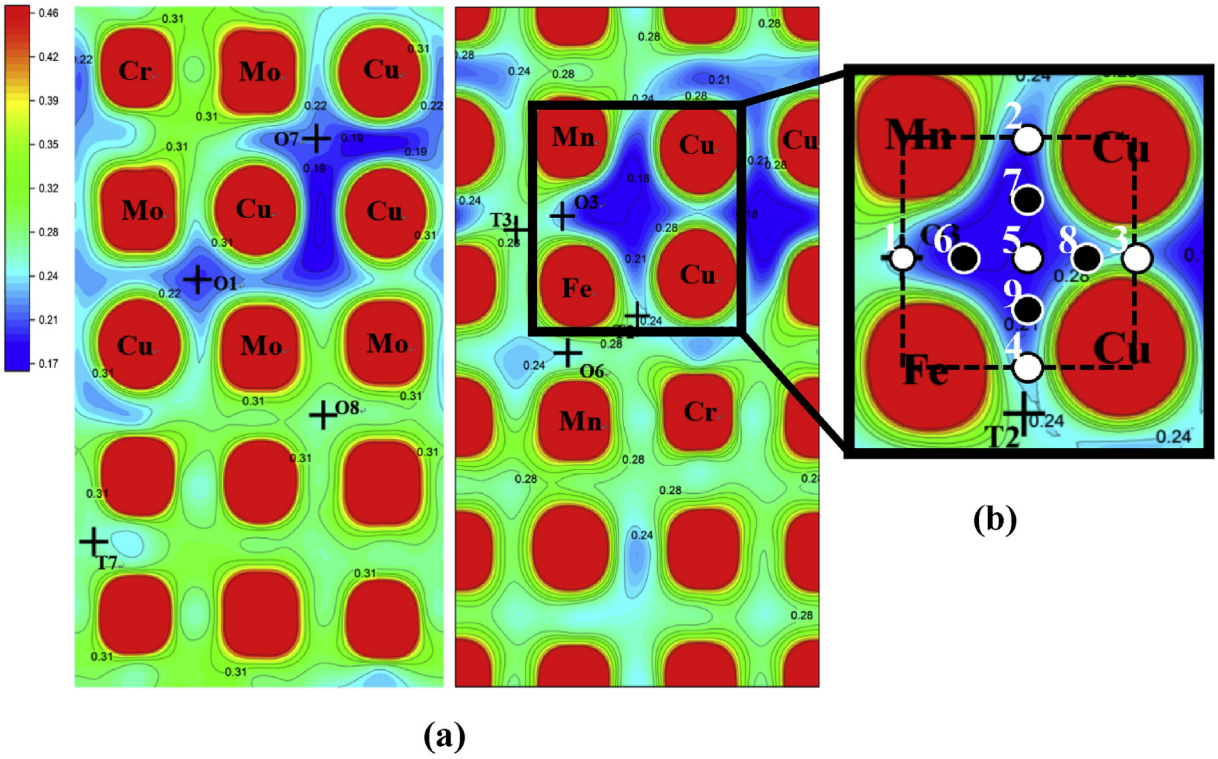

Fig. 2. (a) Electron density of two {100} atomic planes, both including Cu-rich regions. The tetrahedral (I) and octahedral (O) interstitial sites are marked as cross symbols, consistent with those in Fig. 4. (b) A square including a total of nine interstitial positions is magnified in order to clearly show the positions of the interstitials, where the white solid circles are octahedral interstitials (OI) and the black solid circles are tetrahedral interstitials (TI).

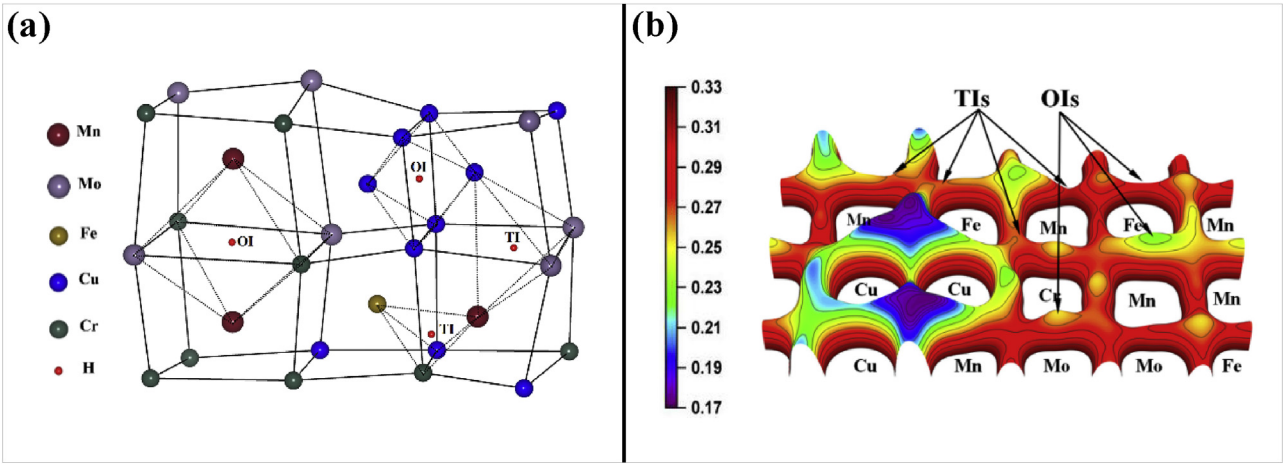

Fig. 3. (a) schematic of the lattice distortion, where distorted OIs and TIs have been outlined. (b) 3D isosurface of electronic density.

and the same free-volume. Thus, the electron density should be a critical variable to influence the solution of H. Therefore, a simple relationship between the solution energy and the electron density can be discovered in simple metals [46]. However, variables to determine the solution of H become much more in HEAs. A detailed analysis showed that the value of the solution energy is caused by the comprehensive effects from the lattice distortion, variation of local chemical environments, and also the destroyed translational symmetry of electronic density.

Statistically, more than half of the interstitial positions are energetically unfavorable for H residing, which is anomalous compared to conventional metals. These unfavorable positions severely limit the long-distance migration of H in HEAs.

When the atoms are arranged in a fully random state, the matrix should exhibit a statistical homogeneity of the chemical environment. When SRO exists in the matrix, segregation of certain species, which suppresses electron mobility, further enhances the electron density fluctuation over the whole matrix. It is instructive to investigate multiple paths of H diffusion in HEAs.

3.4. H diffusion in HEA lattice

For bulk diffusion, H can execute an over-barrier jump under thermal activation [47]. In a BCC lattice, the atomic diffusion coefficient is given by $D = \beta a^2 \Gamma$ according to Einstein's equation, where a is the lattice parameter of the BCC crystal and Γ is the effective

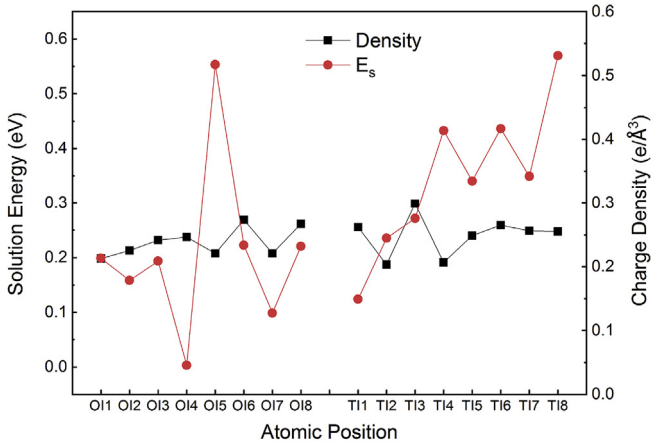

Fig. 4. Relationship between electron density and solution energy. Sixteen of fifty interstitial sites are shown, as arranged along the horizontal axis. Details for all of fifty sites can be seen in Table S2 in the Supplemental Material.

atomic jump frequency depending on the migration style. β is the probability for an interstitial jumping into a new position, dependent on the number of pathways along the migration direction. In BCC lattices, if the interstitial atom jumps via adjacent OIs, β is 1/24. Otherwise, β is 1/48 when jumping is via TIs. Γ is also different for H migration via the TI and the OI positions. The possible paths are summarized in Fig. 5. Recent reports demonstrated that H usually diffuses via adjacent TIs in BCC metals, because TI is a relatively stable position compared to OI [19–22]. Here, both TIs and OIs are considered for jumping, because the energy priority is obscure for H residing. We still refer to Fig. 5 for tracing the H migration to understand the diffusion behavior, in which H jumping between adjacent interstitial positions of different species (here referring to OIs and TIs) is also allowed. Multiple diffusion paths are shown in Fig. 6.

Fig. 6a shows a path along the <100> direction (denoted by Oct <100>). Although OI and TI are arranged alternately along the path (arrowed), H jumps primarily via OI positions because four of five OI sites are energetically stable in this arrow for H residing and the other OI and all the TIs become saddle points. This migration style is not favorable in simple BCC crystals. Along this path, the series

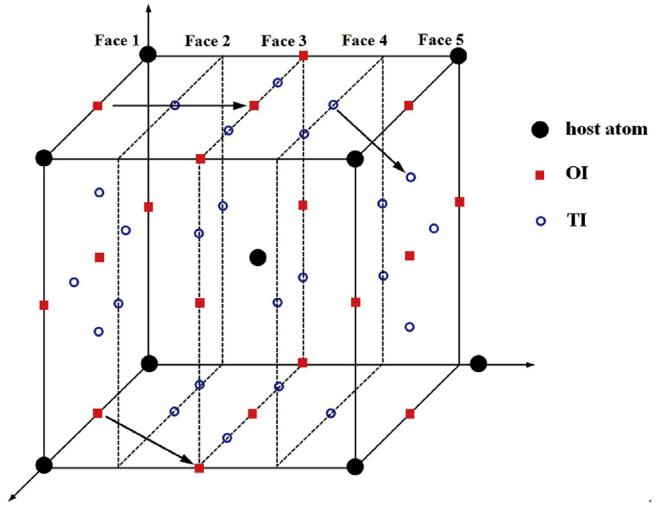

Fig. 5. Schematic view of H jumping via TIs and OIs in the BCC lattice. The arrows denote effective migration pathways.

diffusion barriers setting off from the initial OI site are 0.08, 0.03, and 2.87 eV, respectively. The forward and backward diffusion barriers are totally different. This is a general phenomenon in HEA.

Fig. 6b also shows jumping via OI positions, but along the <110> direction (Oct<110>), which corresponds to octahedral migration in the BCC crystal of Fig. 5. However, the barrier values are not uniform, where the maximum is 2.52 eV, requiring a very high temperature on the order of 900 K to be overcome. Fig. 6c shows the migration just between two adjacent TI positions along the <110> direction (Tet<110>). Although the energy barrier is remarkably small, it is difficult for the H atom to reach distant regions, because the nearby TIs positions lose stability and very few positions can be provided as footholds of H for the next jump. That is to say, migration through adjacent TI positions seldom takes place in the HEA. It can be seen from Fig. 6d, where the jump is between TI positions along the <100> direction (Tet<100>), that the barrier energy from TI_1 to TI_2 is even smaller than the potential energy difference between the two positions, indicating that the H atom is easily trapped in TI_2 and the migration is nonreciprocal.

From the transition state (TS) theory, the effective atomic jump frequency after approximating $\Delta H = \Delta U$ can be derived as [48,49]:

$$\Gamma = \upsilon_0 e^{-E_m/k_B T}, \tag{2}$$

where E_m is the energy barrier, and the vibration frequency (υ_0) is:

$$\upsilon_0 = \prod_i^{3N} \upsilon_i^{\text{initial}} \Big/ \prod_i^{3N-1} \upsilon_i^{\text{saddle}}, \tag{3}$$

$\upsilon_i^{\text{initial}}$ and $\upsilon_i^{\text{saddle}}$ are the atomic vibration frequency of the initial stable structure and saddle structure, respectively, in which the metal atoms were set to be fixed owing to their relatively heavy mass. N equals 1, because only one H atom was considered.

Table 2 lists the rate constants of the aforementioned migration styles, calculated at 300 K using Eqs. (2) and (3), where the counterparts in the α-Fe bulk are shown for comparison. Because W is also a BCC crystal with a similar skeleton to that of the HEA and serves as the first wall subjected to H isotope irradiation in nuclear fusion reactors, we also listed the data of W. Obviously, the effective jump frequency, υ_0, is dominated by E_m, rather than υ_0. For the case of Tet <110>, the rate constant of H jumping forward in the HEA is approximately two orders of magnitude higher than that in W, whereas the reverse jump is one magnitude lower. The ratio of transition frequencies, which can be calculated as $t = \Gamma_{\text{forward}}/\Gamma_{\text{backward}}$, is less than 0.01 for each case, again indicating that the forward and backward migrations do not balance.

4. Discussion

From the results presented above, we can see that the interstitial space is complex in the HEA. The free volume of interstitials in the latter is uniform in conventional metals, whereas it is irregularly diverse in the HEAs. In addition, the density of valence electrons is nonuniform in the interstitial spaces of the HEA, primarily owing to the variable chemical environment. These two factors together diversify the solution energy in the HEA. In particular, the SRO enhances the inhomogeneity of the solution energy. Empirically, if the energy barrier is higher than 0.8 eV, the vibration frequency is too small to overcome the barrier at room temperature. Here, the unstable TI or OI becomes energy barriers, always larger than 0.8 eV. This implies that in the HEA, many effective migration channels are blocked because a number of interstitial positions along the channels are unstable and even become high energy barriers, thereby not assisting the H atom as footholds for further

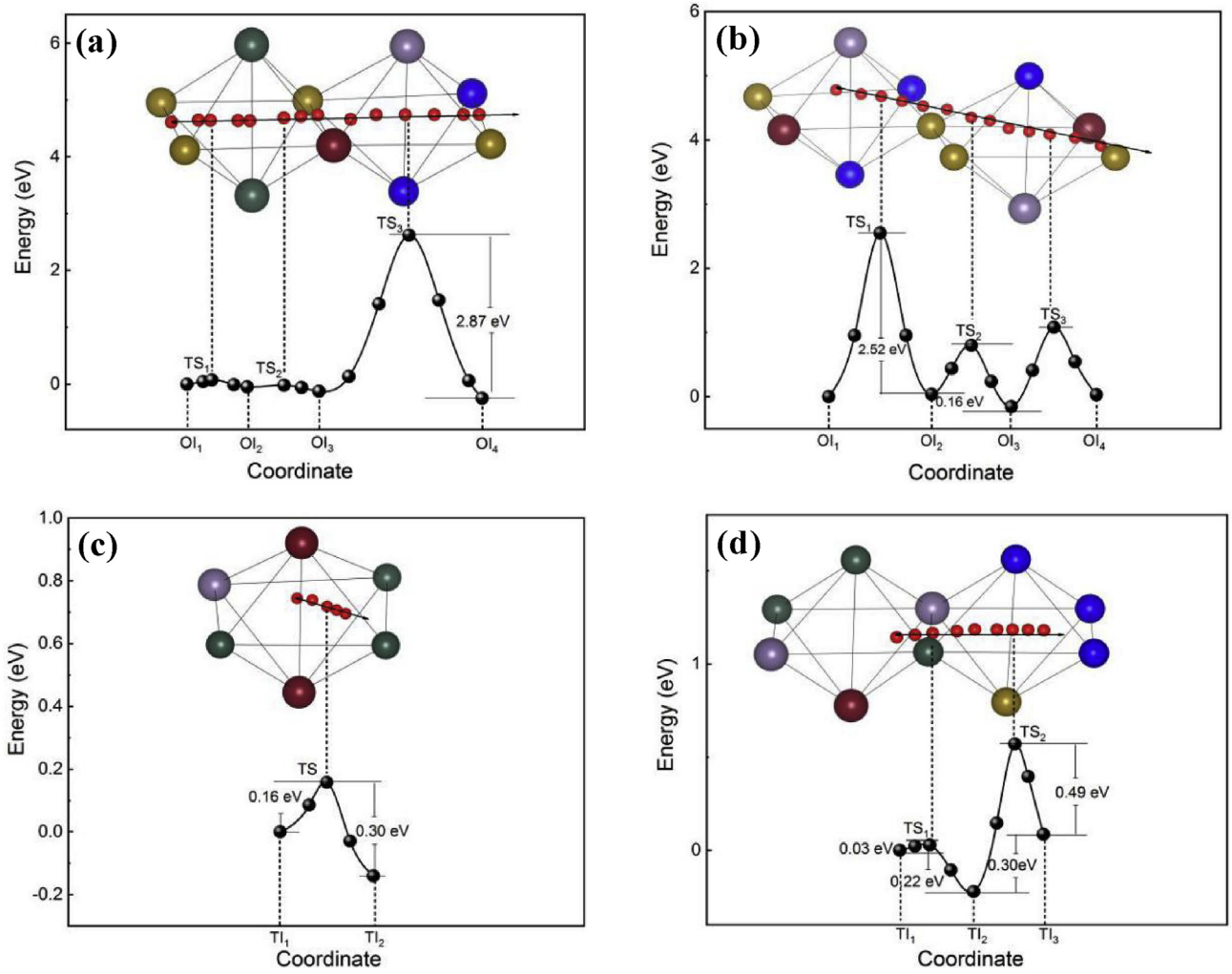

Fig. 6. Energy barriers and transition state (TS) in the diffusion pathways. (a) H hopping via OI positions along the <100> direction, where TS_1 and TS_2 are located at TI positions, and TS_3 is at an OI position; (b) hopping between OIs along the <110> direction; (c) hopping between TIs along the <110> direction; (d) hopping between TIs along the <100> direction, where TS1 and TS2 are located at OIs.

Table 2
Energy barriers, vibration frequencies, and rate constants (at 300 K) along multiple pathways shown in Fig. 6. In the pathway along Tet <100>, TS_2 is a higher order (rank-2) saddle point, with only one real frequency and two imaginary frequencies. The energies in parentheses are the ZPE corrections.

System	Migration style		E_m (eV)	$v_0(10^{12}$ HZ))	Γ(HZ)
HEA	Tet <110>	TI_1-TS (Forward)	0.16 (0.13)	22.2	4.6×10^{10}
		TS-TI_2 (Reverse)	0.30 (0.34)	6.4	5.8×10^{7}
	Oct <110>	OI_2-TS_2 (Forward)	0.76 (0.81)	9.2	1.57×10^{0}
		TS_2-OI_3 (Reverse)	0.95 (0.99)	11.5	1.26×10^{-3}
	Oct <100>	OI_1-TS_1 (Forward)	0.08 (0.05)	51.7	2.34×10^{12}
		TS_1-OI_2 (Reverse)	0.12 (0.09)	2.6	2.5×10^{10}
	Tet <100>	TI_2-TS_2 (Forward)	0.79	–	–
		TS_2-TI_3 (Reverse)	0.48	–	–
α-Fe	Tet<110>		0.164 (0.147)	19.3	3.30×10^{10}
	Ref. [50]		0.142	–	–
W	Tet<110>		0.26 (0.24)	22.2	8.35×10^{8}
	Ref. [20]		0.21	26.2	7.78×10^{9}

jumping. In this situation, the jumping probability β in Einstein's equation is significantly decreased. Actually, it is much more complex to quantify the parameter β and the length for each jumping step in the HEA. In any case, β in the HEA is less than in BCC lattices, leading to a decrease in the diffusion coefficient for HEA.

In simple metals, the energy barriers are distributed periodically, which means that H is capable of diffusing over the lattice once its kinetic energy can overcome the known barrier. However, we do not know the barrier of the next jumping in the HEA if H successfully passes over the current barrier. The diversity of the energy barriers is relatively large in statistics (see the detail in Supplemental Material Fig. S6). To make a quantitative

comparison, the AIMD calculations are carried out to estimate the diffusion coefficients of the HEA.

The trajectory of H atom in bulk materials is shown in Fig. 7. The trajectory of H migration in the HEA is terminated and H will be trapped in a local area with a low probability of escape, in spite of undergoing successive hops (see Fig. 7d). This behavior can be understood from the diverse barriers calculated from CI-NEB (see Fig. 6a–d). By contrast, the movement of H in α-Fe and W enjoys greater freedom. Meanwhile, the diffusion coefficient of H in HEA is smaller than α-Fe and W at different temperatures (see Fig. 8), indicating that H exhibits a slower diffusion in the HEA than those in metals. The energy barriers are obtained from the Arrhenius fitting, as follows: $E^{MD}_{\alpha-Fe} = 0.115eV$, $E^{MD}_{W} = 0.29eV$and $E^{MD}_{HEA} = 0.42eV$. The calculated diffusion barriers of H in α-Fe and W are consistent with the previous calculations [19,51].

The anomalous solution behaviors of H in HEAs result in two remarkable effects on the H diffusivity. First, the diffusion is almost irreversible owing to the large difference in barrier energies for forward and backward jumping. Second, unstable interstitial positions for H residing block the diffusion channels by acting as insurmountable potential saddle points. As a result, H seems to be entangled in a swamp. It is well known that the outstanding properties of HEAs are related to the following "core effects": high entropy, sluggish diffusion, severe lattice distortion, and cocktail effects [11]. For instance, it has been reported that in equiatomic alloys with multiple principal elements, the radiation tolerance can be enhanced owing to the suppression of void formation [7]. This is primarily attributed to the sluggish diffusion of host atoms, which alleviates the generation of supersaturated vacancies. The sluggish effect has been found to originate from the fluctuation in the lattice potential energy [52]. As guest atoms, the H atoms migrate via interstitial positions whose lattice potentials fluctuate, which is responsible for the multiple values of the solution energy of H. Sluggish effects also occur for H, because the energy barriers vary irregularly along the migration pathway, some of which are remarkably high. An additional important factor is that unstable

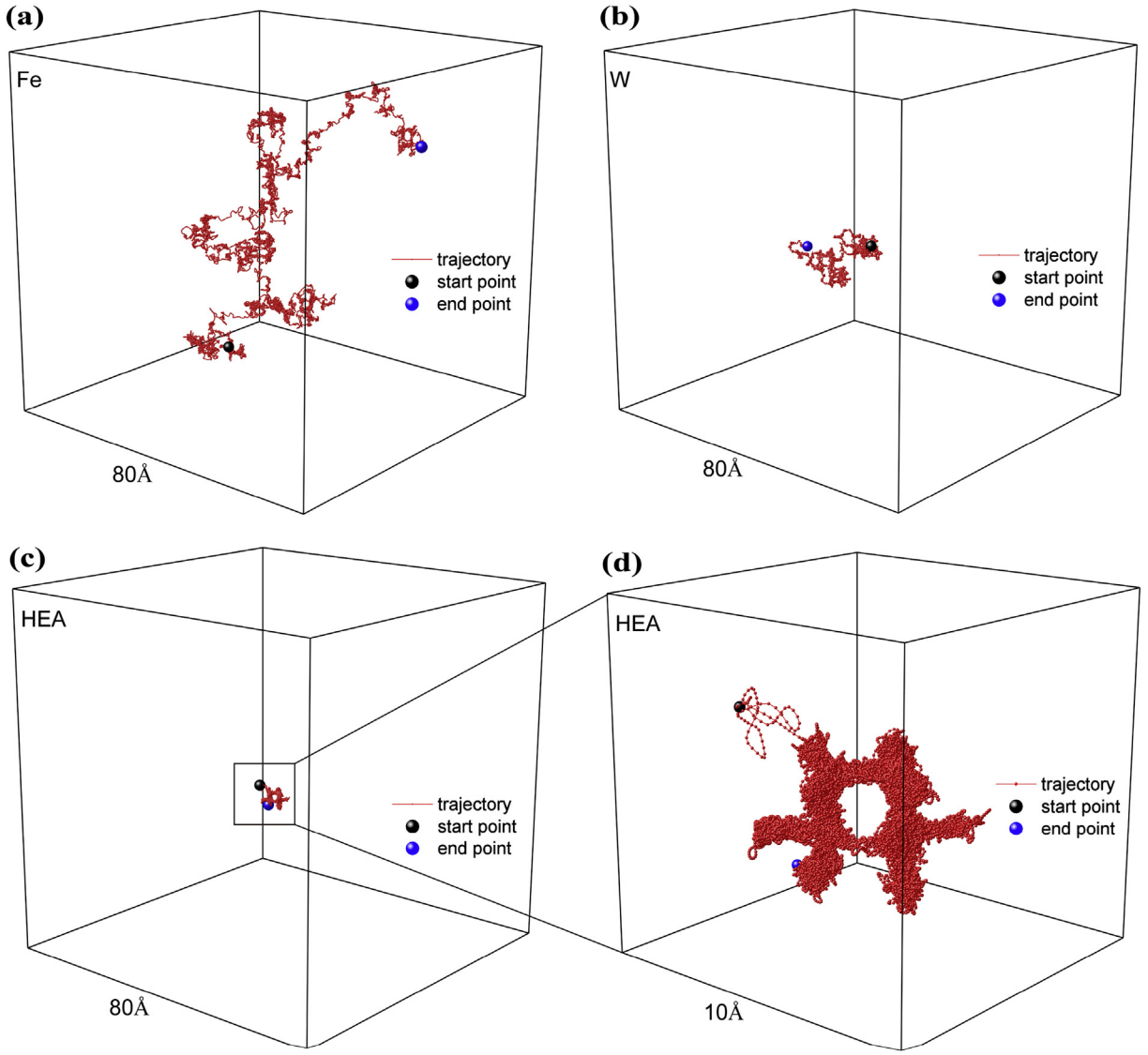

Fig. 7. Trajectories of H atom in bulk materials at 800 K for 0.1 ns. (a) and (b) α-Fe and W bulk with size of 80 Å × 80 Å × 80 Å. (c) HEA bulk with 80 Å × 80 Å × 80 Å. The number of trajectory points is the same in the two bulks; it can be clearly seen that the points are dispersed in α-Fe and concentrated in a local area in HEA. (d) Enlarged image of (c) with a 10 Å × 10 Å × 10 Å cell to illustrate the detailed trajectory of H in HEA. The calculated jump trajectories at 1000 K, 1200 K, and 1500 K are illustrated in Figs. S7–S9 of the Supplemental Material.

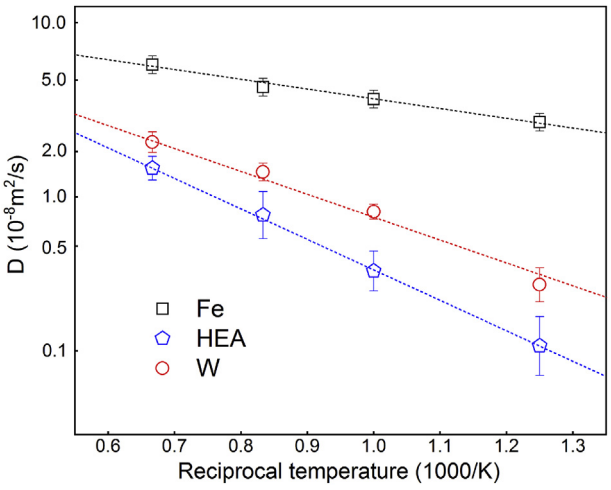

Fig. 8. Diffusion coefficients (D) for the HEA, α-Fe, and W at different temperatures, which were obtained from Einstein relation [10] (see details in Figs. S10–S12 of the Supplemental Materials). The relation between D and the rescaled temperature (T/T_m) is shown in S13.

interstitial positions even block the migration channels of H, which significantly contributes to the sluggish effects, and should not be omitted. This confines H movement in a local region. Combining the two factors, the high mobility of H usually occurring in metals is restricted in the HEAs and diffusion to distant regions is severely retarded. That is to say, the diffusion coefficient of H in the HEA will be intrinsically smaller than that in the corresponding pure metal. This is reflected by the MD calculation (Fig. 7a and c), where the trace of H in α-Fe spreads over the whole simulation cell of 80 Å × 80 Å × 80 Å in 0.1 ns. By contrast, H is still confined in a very small area within the same duration. This mechanism can also rationally interpret the recent experiments in which a near-surface composition gradient of H was observed through the sample thickness of the FeCrNiCoMn HEA [53]. The solution and migration energies of host atoms in concentrated solid solution alloys are also diverse [54,55]. Owing to the unique features of the structure and inherent chemical complexity, retarded diffusion in HEAs should be a common characteristic of atoms, regardless of whether they are the host or the guest.

Because of the high mobility of H in metals, controlling the tritium permeation and reducing tritium losses is a highly intricate problem in fusion reactors (e.g., in water-cooled lithium lead DEMO) and fusion technology. A general scheme for solving these problems was designed to create tritium permeation barriers (TPBs) on the surface of structural components (commonly undertaken by metals) in fusion reactors, with the aim of reducing the tritium leakage [56,57]. For instance, aluminum-rich coatings as TPBs form Al_2O_3 on the surface of structural components. However, the feasibility of this technology relies on the cohesive strength of the interface between the oxide and metals, which is still problematic and has been studied for several years. Recently, it was widely reported that HEAs may be more resistant to radiation damage than the corresponding pure elements [3], particularly in the aspect of suppressing defect cluster growth through defect recombination. Coupled with the findings herein, HEAs would possess comprehensive advantages and are expected to present excellent tolerance to the irradiation of different ions when exposed to hostile nuclear irradiation. In particular, they can be utilized as TPB materials, as the challenges of interface strength would not be involved.

As for traditional metals, FCC austenitic stainless steels and BCC ferritic/martensitic steels, being Fe-based materials, exhibit different properties in irradiation: the FCC steels are good at ductility and fracture toughness, while the BCC steels is superior in mechanical strength and heat resistance. This may be due to discrepancy in their structural characteristics. Whether the structural discrepancy leads to discrepancy of H behavior in FCC and BCC HEAs is still unknown, but is really intriguing.

5. Conclusion

A hybrid method combining DFT with MMC was used to investigate the evolution of H in HEA bulk through systematically calculating the solution energy, migration barriers, and effective jump frequency. We revealed the relationship between the lattice distortion and diffusion properties of H. It was found that the sluggish diffusion, which also occurs for guest light atoms (H) in HEA bulk, is attributed not only to the fluctuation of diffusion barriers originating from the difference between the potential energy of interstitial positions, similar to the cases of host atoms, but also to severe reduction of stable interstitial positions for H residing. Some of these even become insurmountable saddle points and block the long-distance H migration channels. Therefore, the H atoms are easily trapped in low-energy zones (just like swamps) and it is difficult for them to hop out. These swamps surrounded by unstable interstitial positions pervade the whole matrix and remarkably retard long-distance H migration. Considering the high irradiation tolerance of HEAs, the results provide further clues for the successful application of HEAs in the nuclear industry, such as serving as TPBs.

Acknowledgements

This work was supported by the National Natural Science Foundation of China under Grant Nos. 11775051 and 11475046, and the National Key Research and Development Plan Program of China under No. 2017YFA0402503.

Appendix A. Supplementary data

Supplementary data to this article can be found online at https://doi.org/10.1016/j.actamat.2019.09.014.

References

[1] E. Levo, F. Granberg, C. Fridlund, K. Nordlund, F. Djurabekova, Radiation damage buildup and dislocation evolution in Ni and equiatomic multicomponent Ni-based alloys, J. Nucl. Mater. 490 (2017) 323–332.
[2] C. Zlotea, M.A. Sow, G. Ek, J.P. Couzinié, L. Perrière, I. Guillot, J. Bourgon, K.T. Møller, T.R. Jensen, E. Akiba, M. Sahlberg, Hydrogen sorption in TiZrNbHfTa high entropy alloy, J. Alloy. Comp. 775 (2019) 667–674.
[3] F. Granberg, K. Nordlund, M.W. Ullah, K. Jin, C. Lu, H. Bei, L.M. Wang, F. Djurabekova, W.J. Weber, Y. Zhang, Mechanism of radiation damage reduction in equiatomic multicomponent single phase Alloys, Phys. Rev. Lett. 116 (2016) 135504.
[4] N.A.P.K. Kumar, C. Li, K.J. Leonard, H. Bei, S.J. Zinkle, Microstructural stability and mechanical behavior of FeNiMnCr high entropy alloy under ion irradiation, Acta Mater. 113 (2016) 230–244.
[5] G. Velişa, E. Wendler, S. Zhao, K. Jin, H. Bei, W.J. Weber, Y. Zhang, Delayed damage accumulation by athermal suppression of defect production in concentrated solid solution alloys, Mater. Res. Lett. 6 (2017) 136–141.
[6] L.R. Owen, E.J. Pickering, H.Y. Playford, H.J. Stone, M.G. Tucker, N.G. Jones, An assessment of the lattice strain in the CrMnFeCoNi high-entropy alloy, Acta Mater. 122 (2017) 11–18.
[7] C. Lu, L. Niu, N. Chen, K. Jin, T. Yang, P. Xiu, Y. Zhang, F. Gao, H. Bei, S. Shi, M.R. He, I.M. Robertson, W.J. Weber, L.M. Wang, Enhancing radiation tolerance by controlling defect mobility and migration pathways in multicomponent single-phase alloys, Nat. Commun. 7 (2016) 13564.
[8] S. Zhao, G. Velisa, H. Xue, H. Bei, W.J. Weber, Y. Zhang, Suppression of vacancy cluster growth in concentrated solid solution alloys, Acta Mater. 125 (2017) 231–237.
[9] B. Gludovatz, A. Hohenwarter, K.V. Thurston, H. Bei, Z. Wu, E.P. George, R.O. Ritchie, Exceptional damage-tolerance of a medium-entropy alloy CrCoNi

at cryogenic temperatures, Nat. Commun. 7 (2016) 10602.
[10] S. Zhao, Y. Osetsky, Y. Zhang, Preferential diffusion in concentrated solid solution alloys: NiFe, NiCo and NiCoCr, Acta Mater. 128 (2017) 391–399.
[11] J.W. Yeh, S.K. Chen, S.J. Lin, J.Y. Gan, T.S. Chin, T.T. Shun, C.H. Tsau, S.Y. Chang, Nanostructured high-entropy alloys with multiple principal elements: novel alloy design concepts and outcomes, Adv. Eng. Mater. 5 (2004) 6.
[12] M. Vaidya, K.G. Pradeep, B.S. Murty, G. Wilde, S.V. Divinski, Bulk tracer diffusion in CoCrFeNi and CoCrFeMnNi high entropy alloys, Acta Mater. 146 (2018) 211–224.
[13] M. Vaidya, S. Trubel, B.S. Murty, G. Wilde, S.V. Divinski, Ni tracer diffusion in CoCrFeNi and CoCrFeMnNi high entropy alloys, J. Alloy. Comp. 688 (2016) 994–1001.
[14] A.R. Allnatt, T.R. Paul, I.V. Belova, G.E. Murch, A high accuracy diffusion kinetics formalism for random multicomponent alloys: application to high entropy alloys, Philos. Mag. 96 (2016) 2969–2985.
[15] C. Ng, S. Guo, J.H. Luan, S.Q. Shi, C.T. Liu, Entropy-driven phase stability and slow diffusion kinetics in an Al0.5CoCrCuFeNi high entropy alloy, Intermetallics 31 (2012) 165–172.
[16] V.K. Alimov, J. Roth, M. Mayer, Depth distribution of deuterium in single- and polycrystalline tungsten up to depths of several micrometers, J. Nucl. Mater. 337–339 (2005) 619–623.
[17] M. Poon, R.G. Macaulay-Newcombe, J.W. Davis, A.A. Haasz, Effects of background gas impurities during D+ irradiation on D trapping in single crystal tungsten, J. Nucl. Mater. 337–339 (2005) 629–633.
[18] P.G. Sundell, G. Wahnström, Self-trapping and diffusion of hydrogen in Nb and Ta from first principles, Phys. Rev. B 70 (2004).
[19] D.E. Jiang, E.A. Carter, Diffusion of interstitial hydrogen into and through bcc Fe from first principles, Phys. Rev. B 70 (2004).
[20] K. Heinola, T. Ahlgren, Diffusion of hydrogen in bcc tungsten studied with first principle calculations, J. Appl. Phys. 107 (2010).
[21] J. Luo, H.B. Zhou, Y.L. Liu, L.J. Gui, S. Jin, Y. Zhang, G.H. Lu, Dissolution, diffusion and permeation behavior of hydrogen in vanadium: a first-principles investigation, J. Phys. : Condens. Matter 23 (2011), 135501.
[22] D.F. Johnson, E.A. Carter, Hydrogen in tungsten: absorption, diffusion, vacancy trapping, and decohesion, J. Mater. Res. 25 (2011) 315–327.
[23] Y. Zhang, G.M. Stocks, K. Jin, C. Lu, H. Bei, B.C. Sales, L. Wang, L.K. Beland, R.E. Stoller, G.D. Samolyuk, M. Caro, A. Caro, W.J. Weber, Influence of chemical disorder on energy dissipation and defect evolution in concentrated solid solution alloys, Nat. Commun. 6 (2015) 8736.
[24] Z.H. Zhong, Q. Xu, K. Mori, M. Tokitani, Thermal stability of microstructures and mechanical properties in a Fe-based Fe-Cr-Mn-Cu-Mo multi-component alloy, Philos. Mag. 99 (2019) 1515.
[25] L.J. Santodonato, Y. Zhang, M. Feygenson, C.M. Parish, M.C. Gao, R.J. Weber, J.C. Neuefeind, Z. Tang, P.K. Liaw, Deviation from high-entropy configurations in the atomic distributions of a multi-principal-element alloy, Nat. Commun. 6 (2015) 5964.
[26] A. Tamm, A. Aabloo, M. Klintenberg, M. Stocks, A. Caro, Atomic-scale properties of Ni-based FCC ternary, and quaternary alloys, Acta Mater. 99 (2015) 307–312.
[27] G., M. Bracq, Laurent-Brocq, L. Perrière, P. Pirès, J.M. Joubert, I. Guillot, The fcc solid solution stability in the Co-Cr-Fe-Mn-Ni multi-component system, Acta Mater. 128 (2017) 327–336.
[28] S.H. Wei, L.G. Ferreira, J.E. Bernard, A. Zunger, Electronic properties of random alloys: special quasirandm structures, Phys. Rev. B 42 (1990) 15.
[29] F. Tian, A review of solid-solution models of high-entropy alloys based on ab initio calculations, Front. Mater. 4 (2017).
[30] Prashant Singh, A.V. Smirnov, D.D. Johnson, Atomic short-range order and incipient long-range order in high-entropy alloys, Phys. Rev. B 91 (2015) 224204.
[31] N. Metropolis, A.W. Rosenbluth, M.N. Rosenbluth, A.H. Teller, E. Teller, Equation of state calculations by fast computing machines, J. Chem. Phys. 21 (1953) 1087–1092.
[32] Y.X. Wang, M. Hou, Ordering of bimetallic nanoalloys predicted from bulk alloy phase diagrams, J. Phys. Chem. C 116 (2012) 10814–10818.
[33] C. Niu, Y, Rao, W, Windl, M. Ghazisaeidi, Multi-Cell Monte Carlo Method for Phase Prediction, arXiv preprint arXiv 1811 (2018) 04092.
[34] M.A. Zagrebin, V.V. Sokolovskiy, V.D. Buchelnikov, Ab initio calculations of structural and magnetic properties of Ni-Co-Mn-Cr-Sn supercell, Intermetallics 87 (2017) 55–60.
[35] C. Niu, W. Windl, M. Ghazisaeidi, Multi-cell Monte Carlo relaxation method for predicting phase stability of alloys, Scr. Mater. 132 (2017) 9–12.
[36] A. van de Walle, P. Tiwary, M. de Jong, D.L. Olmsted, M. Asta, A. Dick, D. Shin, Y. Wang, L.Q. Chen, Z.K. Liu, Efficient stochastic generation of special quasirandom structures, Calphad 42 (2013) 13–18.
[37] D. Sheppard, P. Xiao, W. Chemelewski, D.D. Johnson, G. Henkelman, A generalized solid-state nudged elastic band method, J. Chem. Phys. 136 (2012), 074103.
[38] M.S. Hooshmand, C. Niu, D.R. Trinkle, M. Ghazisaeidi, First-principles prediction of oxygen diffusivity near the (102) twin boundary in titanium, Acta Mater. 156 (2018) 11–19.
[39] G. Henkelman, B.P. Uberuaga, H. Jónsson, A climbing image nudged elastic band method for finding saddle points and minimum energy paths, J. Chem. Phys. 113 (2000) 9901–9904.
[40] J.M. Cowley, An approximate theory of order in alloys, Phys. Rev. 77 (1950) 669–675.
[41] S. Singh, N. Wanderka, B.S. Murty, U. Glatzel, J. Banhart, Decomposition in multi-component AlCoCrCuFeNi high-entropy alloy, Acta Mater. 59 (2011) 182–190.
[42] E.A. Brandes, G.B. Brook, 7th Smithells Metals Reference Book, 1992.
[43] S.J. Zhao, T. Egami, G.M. Stocks, Y.W. Zhang, Effect of d electrons on defect properties in equiatomic NiCoCr and NiCoFeCr concentrated solid solution alloys, Phys. Rev. Mater. 2 (2018), 013602.
[44] M.J. Puska, R.M. Nieminen, M. Manninen, Atoms embedded in an electron gas: immersion energies, Phys. Rev. B 24 (1981) 3037–3047.
[45] H.-B. Zhou, Y.-L. Liu, S. Jin, Y. Zhang, G.N. Luo, G.-H. Lu, Investigating behaviours of hydrogen in a tungsten grain boundary by first principles: from dissolution and diffusion to a trapping mechanism, Nucl. Fusion 50 (2010).
[46] J. Nørskov, F. Besenbacher, J. Bøttiger, B.B. Nielsen, A. Pisarev, Interaction of hydrogen with defects in metals: interplay between theory and experiment, Phys. Rev. Lett. 49 (19) (1982) 1420–1423.
[47] G. Alefeld, J. Volkl, Hydrogen in Metals I Basic Properties, 1978.
[48] M. Mantina, Y. Wang, R. Arroyave, L.Q. Chen, Z.K. Liu, C. Wolverton, First-principles calculation of self-diffusion coefficients, Phys. Rev. Lett. 100 (2008) 215901.
[49] M. Mantina, Y. Wang, L.Q. Chen, Z.K. Liu, C. Wolverton, First principles impurity diffusion coefficients, Acta Mater. 57 (2009) 4102–4108.
[50] R. Wagner, R. Sizmann, Die Diffusion und Permeation von Wasserstoff in alpha-Eisen, Z. Angew. Phys. 18 (1964) 193.
[51] J. Sanchez, J. Fullea, M.C. Andrade, P.L. de Andres, Ab initio molecular dynamics simulation of hydrogen diffusion in α-iron, Phys. Rev. B 81 (2010) 132102.
[52] K.Y. Tsai, M.H. Tsai, J.W. Yeh, Sluggish diffusion in Co–Cr–Fe–Mn–Ni high-entropy alloys, Acta Mater. 61 (2013) 4887–4897.
[53] H. Luo, W. Lu, X. Fang, D. Ponge, Z. Li, D. Raabe, Beating hydrogen with its own weapon: nano-twin gradients enhance embrittlement resistance of a high-entropy alloy, Mater. Today 21 (2018) 1003–1009.
[54] S. Zhao, G.M. Stocks, Y. Zhang, Defect energetics of concentrated solid-solution alloys from ab initio calculations: $Ni_{0.5}Co_{0.5}$, $Ni_{0.5}Fe_{0.5}$, $Ni_{0.8}Fe_{0.2}$ and $Ni_{0.8}Cr_{0.2}$, Phys. Chem. Chem. Phys. 18 (2016) 24043–24056.
[55] J.B. Piochaud, T.P.C. Klaver, G. Adjanor, P. Olsson, C. Domain, C.S. Becquart, First-principles study of point defects in an fcc Fe-10Ni-20Cr model alloy, Phys. Rev. B 89 (2014), 024101.
[56] A. Aiello, A. Ciampichetti, G. Benamati, An overview on tritium permeation barrier development for WCLL blanket concept, J. Nucl. Mater. 329–333 (2004) 1398–1402.
[57] A. Aiello, G. Benamati, M. Chini, C. Fazio, E. Serra, Z. Yao, Hydrogen permeation through tritium permeation barrier in Pb–17Li, Fusion Eng. Des. 58–59 (2001) 737–742.